Single-Mode Fiber Connector Using Core-Centered Ferrules

GIOK-DJAN KHOE, MEMBER, IEEE, JOHANNES H.F.M. VAN LEEST, AND JOHANNES A. LUIJENDIJK

Abstract—**Fiber connectors using single-mode fibers have been fabricated with an average connection loss of 0.32 dB without index matching. All dimensions of the connector parts, including those of the ferrules and fibers require only low precision. A special lathe is used, in a simple operation, to eliminate the errors of the ferrule-terminated fiber assembly.**

I. Introduction

With the growing interest being shown in single-mode fibers, the importance of designing a low-loss simple plug-in connector for these fibers is evident. Present designs [1], [2] are usually based on high-precision fibers with excellent geometrical properties. All parts used to support the fiber, such as capillaries and ferrules, also require high precision. Precision parts are not required in lens connectors [7], but these designs obviously require the use of lenses and parts for the attachment and adjustment.

We present a detailed description of a new single-mode fiber connector based on a butt-joint between two ferrule-terminated fiber ends. Poor dimensional accuracy of all parts of the connector is allowed in this design. This includes the geometrical properties of the fiber such as the eccentricity of the core and the diameter of the cladding. The geometrical errors of the assembled ferrules are eliminated with the help of a special lathe. Details of the design and operation of this lathe are presented.

Experimental results show that the connectors can be fabricated easily with very low concentration losses. Optical contact between the polished fiber end faces, which results in the reduction of Fresnel reflection losses [3], contributes to the low value of average connection loss.

II. Fiber End Preparation

Fig. 1 shows a ferrule-terminated fiber end. The ferrule is assembled in the following order. The fiber is first glued in the capillary and the capillary is then glued in the metal ferrule. Finally, the fiber end is polished together with the supporting glass capillary and a small rim of the ferrule. In this stage the eccentricity of the fiber core with respect to the ferrule surface may still be as much as 100 μm. It is therefore possible to fabricate the capillaries and ferrules using common workshop methods.

Capillaries for this purpose are drawn from Pyrex preforms. These preforms are commercial tubes with a hole of approximately 0.5 mm. For the present design, the preforms are drawn to form capillaries with a hole diameter between 130 and 140 μm. The outer diameter is approximately 1.8 mm. Finally, the capillaries are cut into pieces of 10 mm. For easy insertion of the fiber during assembly, the capillaries are provided with a funnel-shaped end on one side. This funnel shape is fabricated in the following way. First, the outer surface of the capillaries is covered with shellac. Then one end of the tubes is immersed in a solution of 40 percent HF for about 30 min. The shellac is finally removed using ethanol. Funnel shapes with a depth of approximately 2 mm and an opening of 0.5 mm in diameter are created in this way.

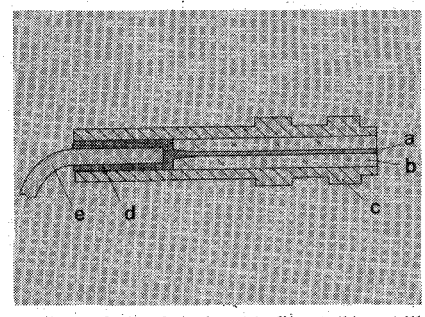

Fig. 1. Cross section of the ferrule: (a) fiber; (b) capillary; (c) metal ferrule with two rings; (d) epoxy; (e) jacket. The front surface is polished. The diameter of the rings is 4.95 before being turned with the lathe. The lathe cuts the rings to 4.700 mm.

To prevent wear of the diamond cutter in the special lathe, it is necessary to use nonferrous metals for the ferrules. A variety of nonferrous alloys are commercially available. For the present experiments we used brass, phosphorbronze, and ARCAP AP1D, an alloy supplied by ARCAP A.G., Switzerland.

The front surface of the ferrule is polished and lapped in two steps. Abrasive plastic sheets are used for this purpose. The first sheet is coated with 23 μm silicon carbide and the second sheet is coated with 1 μm alumnium oxide. Both steps take about 10 s each. Water is continuously poured over the sheets during the polishing and lapping process to make sure that loose particles are washed away. Fig. 2 shows an SEM photograph and an interferogram of a polished ferrule end. Fig. 3 shows a measurement of the surface quality using a Talysurf, a Rank Taylor-Hobson surface texture measuring instrument. The scan was repeated on various other samples and paths over the surface with similar results. The Talysurf scans and interferograms show that the polished surface is slightly convex. The quality and shape of the polished surface allows optical contact between the fiber end faces in the connector, which results in connection losses lower than 0.36 dB without using index matching material [3].

The ferrule is now ready for preparation with the special lathe. At this stage, the core of the single-mode fiber is not yet at the center of the ferrule.

Manuscript received February 22, 1982.
The authors are with Philips Research Laboratories, Eindhoven, The Netherlands.

0018-9480/82/1000-1561$00.75

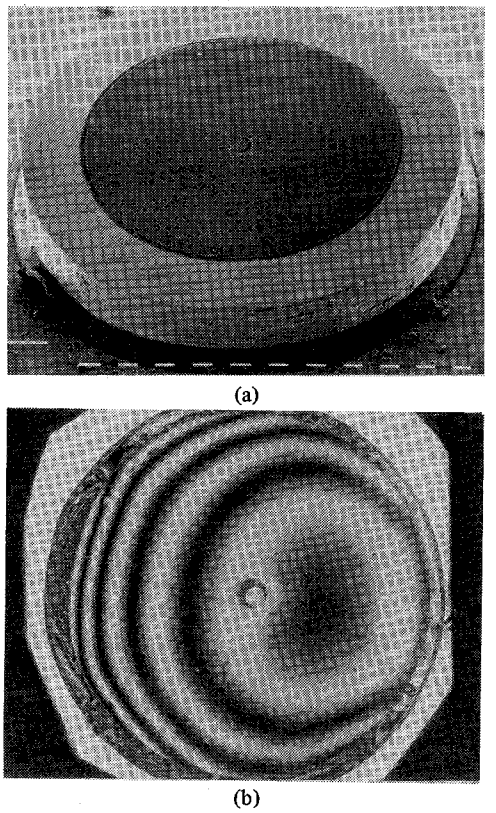

Fig. 2. Photographs of the polished end surface. (a) SEM picture showing various portions of the polished surface. (b) Interferogram of the surface of the capillary and fiber showing a slightly convex profile.

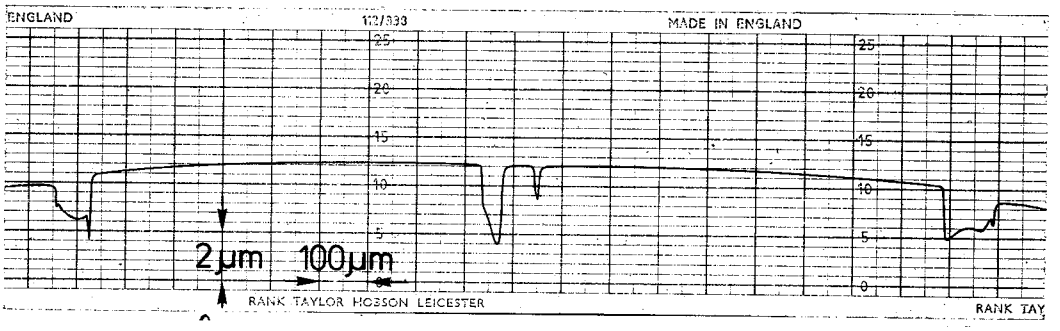

Fig. 3. Talysurf scan of the surface also showing a convex surface.

III. The Lathe

The final accuracy of the ferrules is achieved by means of a lathe, with which two rings near the front end of the ferrule can be turned. The purpose of this operation is to make these rings concentric with respect to the fiber core to within 0.1 μm despite the original excentricity of, for example, 100 μm. The operation is explained in Fig. 4 and consists of the following steps.

1) The ferrule is clamped in the lathe.

2) The other fiber end is illuminated by a suitable light source.

3) The ferrule mount is moved in such a way that the axis of the fiber core coincides with the axis of rotation of the lathe. A special optical system [4] inside the lathe enables the operator to perform this step with an accuracy to within 0.1 μm.

4) The two rings are turned.

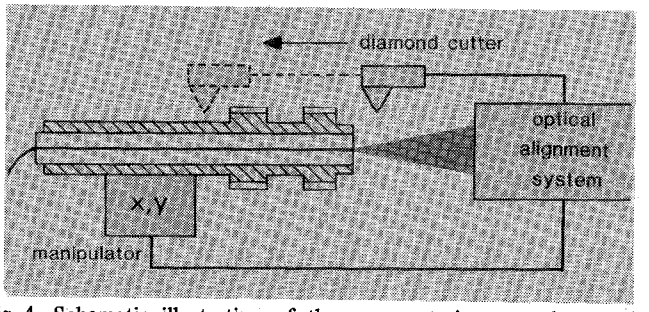

Fig. 4. Schematic illustration of the core-centering procedure. The diamond cutter, optical system, and manipulator are parts of the special lathe.

5) Angular misalignment of the optical beam of the fiber can be detected during the turning step.

The complete procedure takes less than 2 min.

It is obvious that the above-mentioned precision cannot be

obtained with the aid of straightforward optical methods such as adjusting the near field of the core to a reference.

A. Optical System

We designed a novel optical system which is illustrated in Fig. 5. The monomode fiber is illuminated from the other end with a lens-coupled laser diode [5]. About 0.1 mW of the laser light must be coupled into the fiber for the present system, which is obviously simple to realize. A 32X microscope objective is used to create an image of the near field on a camera tube, at a distance of about 35 cm from this lens. The present objective is a Leitz UM type which allows a separation of about 16 mm between the fiber end and the lens. A small spot will now be visible on the monitor.

If all relevant components are perfectly aligned, the spot will not move, if the lathe, including the lens, is rotating [Fig. 5(a)]. When the lens is deliberately misaligned with respect to the axis of rotation, a ring will be visible on the monitor [Fig. 5(b)]. Next, a beamsplitting device is inserted in such a way that the light beam is separated into two parts. The distance of the images to the axis of the lathe is deliberately made unequal, so that two separate rings will be displayed on the monitor when the lathe, including all optical components, is rotating. The beamsplitting device is a combination of a beamsplitting cube and a penta prism, as shown in Fig. 5(c).

If the fiber core is properly adjusted to the axis of the lathe, two concentric rings will be displayed. Any other position of the core will result in nonconcentric rings. The diameters of the rings are adjusted in such a way that only a very thin dark ring separates the illuminated areas when the core is properly aligned. This pattern is shown in Fig. 6(a). Very small deviations in the dark ring can easily be detected by the operator of the machine. Fig. 6(b) shows nonconcentric rings originating from a core which is shifted 1 μm away from the required position.

Persons not trained in the art can adjust the core with an accuracy of at least 0.1 μm. Skilled personnel can adjust easily with errors less than 0.05 μm. These numbers are confirmed by coupling microdisplacement meters to the ferrule mount. The operators could not see the display of the meters and had to adjust the core by observing the ring patterns only.

The following features contribute to the accuracy of the method. When the core is shifted from the proper position, the two light rings on the monitor will move in the opposite direction, as can clearly be seen in Fig. 5(d). Another important reason is that the human eye is very sensitive to detecting deviations in the concentricity of closely separated rings.

The same optical system is used to check the direction of the light beam coming out of the core in the following way. When the rotating part of the lathe starts to move axially for the turning process, the optical system will move accordingly towards the ferrule. Reduction in the distance between the lens and core surface will cause blurring of the picture of the monitor. The blurred pattern on the monitor will stay at its original position if the axis of the light beam is aligned to that of the lathe. Angular misalignment of the light beam will cause the blurring pattern to move away from its original position. The operator will stop the lathe immediately if a movement is detected. Experiments have shown that a common operator can detect an angular misalignment of 0.3°.

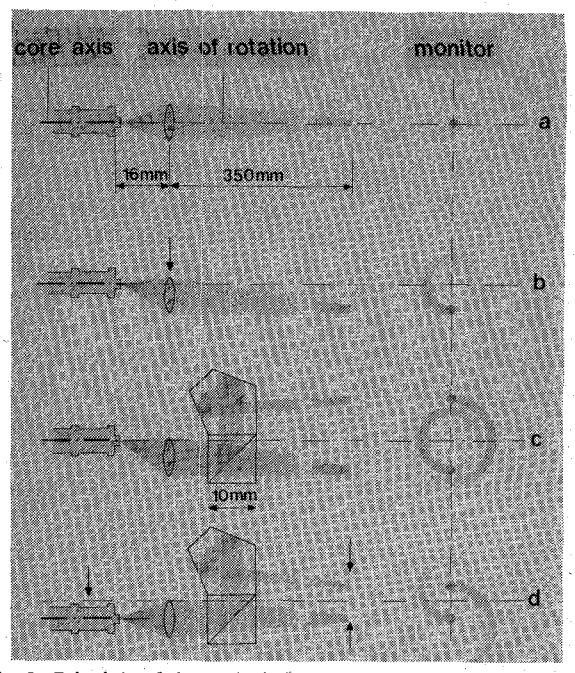

Fig. 5. Principle of the optical alignment system inside the lathe.

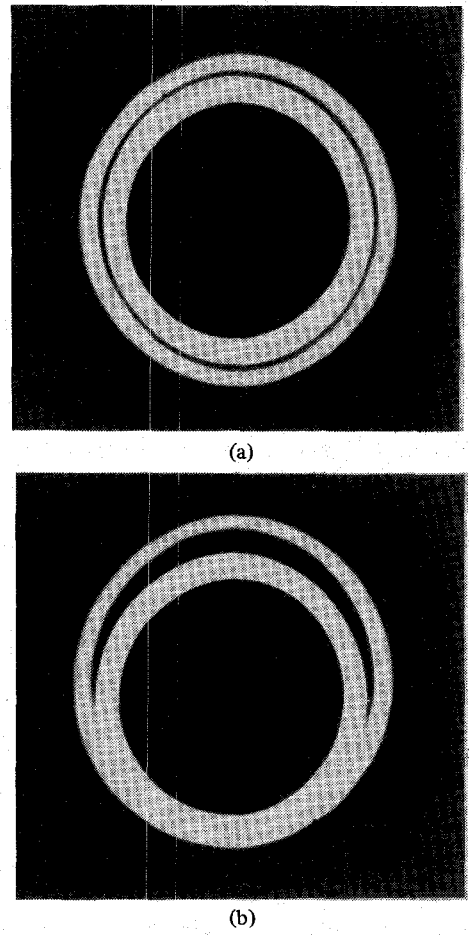

(a) (b)

Fig. 6. Ring patterns as can be seen on the monitor. (a) Fiber core properly aligned. (b) Fiber core moved 1 μm away from the previous position.

Angular misalignment can be caused by several errors. The ferrule can be improperly clamped in the mount due to, for example, a burr on the ferrule surface. In this case, the ferrule can be turned properly after removal of the burr.

B. Mechanical System

The most exacting task of the lathe is to eliminate the concentricity errors of the fiber core to the cylindrical surface of the ferrule. An important requirement of the bearing for this application is the ability to accurately define the axis of rotation of the shaft of the lathe. With respect to axis definition, the aerostatic bearing, also called the externally pressurized bearing, has no equal [6] and is therefore chosen for the present design. Radial support for the rotating shaft of the lathe is provided by a journal bearing and the axial location of the same shaft is provided by a thrust bearing [6].

A simplified cross section of the lathe is shown in Fig. 7. The rotating part of the bearing is a hollow shaft (t) containing various cavities. These cavities are used to accommodate the optical components, the diamond cutter (c), and various mechanical parts for the mounting and adjustment of those components. The bearing gap is conical. A spacing of 10 μm is present between the shaft and the bearing bush at both open ends of the gap. This gap gradually increases to 30 μm at the middle. This is the place where pressurized air is injected into the bearing through a single hole in the bush. The orifice of the air feed hole is extended all around the middle of the bush to create a circumferential air pocket (h). This air pocket is used instead of a radial row of air inlets. Pressurized air flows through the single feed hole into the pocket and then axially to both open ends of the gap where it exhausts to the atmosphere.

The vertical shaft is prevented from sliding downwards by a pivot (p) at the lower end. An aerostatic thrust bearing is used here to separate the pivot from the rotating shaft. Axial movement of the rotating shaft for the turning procedure is obtained by moving the pivot upwards. The zero set of the same pivot is used to set the proper distance between the lens and the core surface of the fiber.

Measurements show that the lathe has a stability of 50 N/μm against transverse load, using an external air pressure of 6 atm. The maximum load measured at the diamond tip during a cutting process was found to be less than 1 N, which is well within the required limits. The present machine consumes 0.01 m^3/min air during operation. Supply of pressurized air is simply shut off when the machine is not in use. Aerostatic bearings exhibit by far the lowest friction torque and can therefore be driven by simple low-torque motors (m). A rubber belt (n) is used to connect the pulley of the motor to that of the shaft. The belt is a simple O ring.

Another important feature of the machine is that it accommodates stable and accurate means for the adjustment of the diamond and the optical components. The distance between the diamond tip and the axis can be set with the aid of a fine adjustment screw. One revolution of the screw corresponds to 3 μm of travel of the diamond tip. A radial adjustment is also provided in the lens mount. This adjustment is used to set the diameter of the inner light ring on the monitor. Finally, the gap between the two rings can be set by tilting the prism assembly. Special attention was paid to the construction of this tilting mechanism because the gap setting is very important for the use of the machine. The construction is shown schematically in Fig. 7. A tube is placed inside the hollow shaft. The prism assembly is mounted at the upper end of this tube which is fixed to the shaft by a thick membrane spring. The radial position of the lower end of this tube can be varied with respect to the shaft by using suitable screws. A stable and fine adjustment of the prisms is obtained in this way.

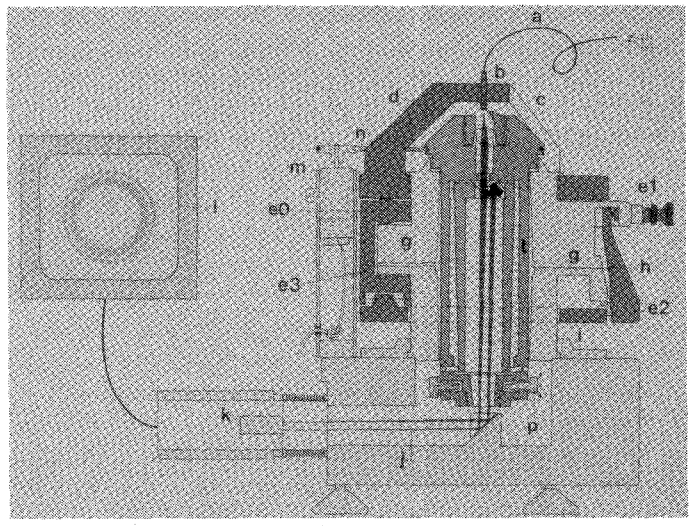

Fig. 7. Simplified cross section of the lathe: (a, b) ferrule with pigtail; (t) rotating shaft containing the optical system; (g, h) bearing bush and air pocket with one inlet shown on the left side; (c) diamond mounted on the shaft; (d, $e0$, $e1$, $e2$, $e3$, i) manipulator consisting of a tripod, a ball, a microspindle, and various links; (j, k, l) optical path, camera, and monitor; (m, n) motor and belt; (p) pivot.

Finally, a stable and accurate manipulator must be provided to adjust the ferrule to the desired position. The manipulators must be able to maintain the position of the ferrule during the turning process. In the present design, the ferrule is mounted on a tripod (d) which is spring loaded with 600 N on three 20 mm steel balls ($e0$). The tripod will move with respect to the frame of the machine if the balls are rolled. A system of links and deformable joints is then used to transfer movements of two microspindles ($e1$) into a rolling movement of the balls. A travel of 56 μm of the microspindle is translated into a reduced travel of 1 μm of the tripod. The manipulator system is indicated in Fig. 7.

IV. Core-Centered Ferrules

Several batches of ferrules were turned with the aerostatic lathe to examine the performance of the machine. A photograph of the lathe is shown in Fig. 8(a). The binocular seen in front of the machine is part of a stereo microscope used to observe the ferrule and the diamond chisel. Part of the tripod, ferrule, and the diamond is seen in Fig. 8(b).

Wear of the diamond chisel is not observed as long as nonferrous metals are used for the ferrule. Variations in the diameter of the nonferrous ferrules are less than 0.05 μm if the ferrules are turned twice. Turning the ferrules for the third time has no measurable influence on the geometry. A dummy cylinder of the same material is turned with the lathe before turning a batch of pigtailed ferrules to check the diameter setting.

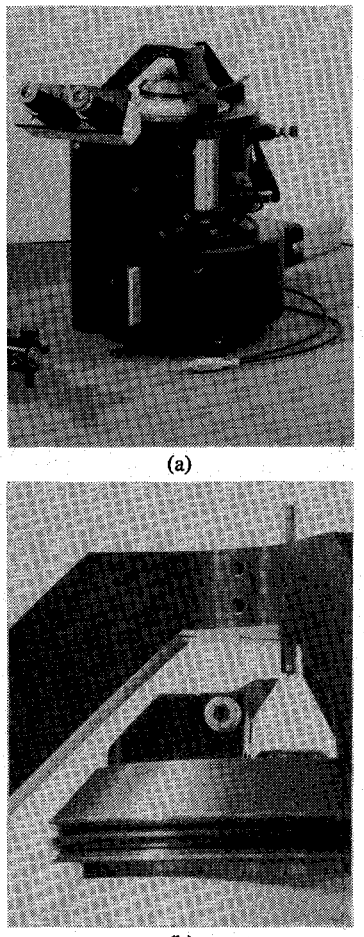

(a)

(b)

Fig. 8. Photographs of the lathe. (a) Overall view. (b) Close-up showing the diamond and ferrule. The machine has a height of 40 cm.

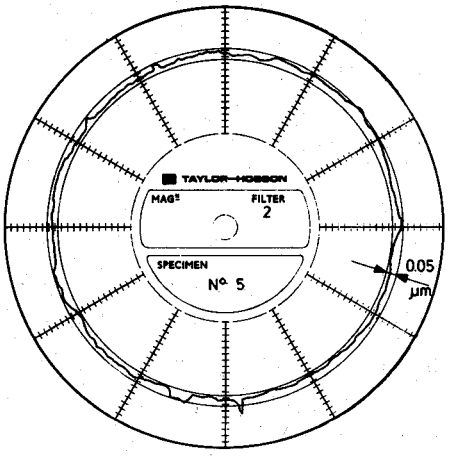

Fig. 9. Circularity of a turned ring measured with a talyrond.

Circularity of the turned surface of the ferrules was measured with a talyrond. Measured circularities were found to be within 0.05 μm. One of the measured curves is shown in Fig. 9.

The high quality of the ferrules is clearly demonstrated by coupling loss measurements in a V-groove. A histogram of coupling losses is shown in Fig. 10(a). The second histogram in Fig. 10(b) shows coupling losses of the same pairs of ferrules, but in addition, one of the two ferrules was rotated in steps of 60° and the losses were measured in each of the new positions. The third histogram of Fig. 10(c) shows the measured difference between the maximum losses and minimum losses for each pair of ferrules in the previous test. We note that the ferrules are inserted and clamped in the V-groove by hand-operated levers. The results are therefore slightly dependent on the operator. Repetition of the same situation can result in a deviation of maximum 0.1 dB from the original value. Results presented in the next section are obtained with the connector and are not influenced by the operator, but depend on the operation of the spring systems.

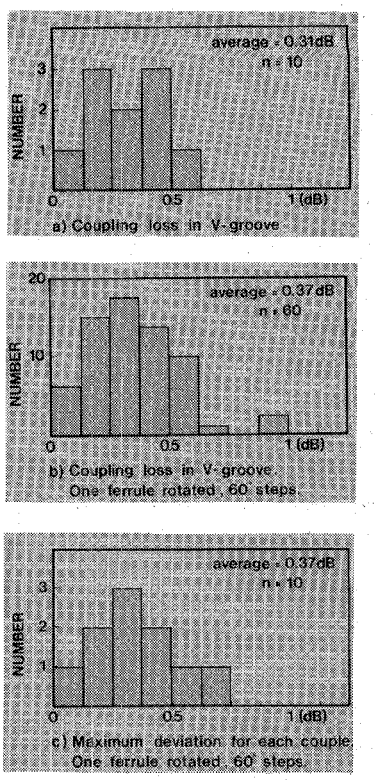

Fig. 10. Connection loss of the turned ferrules measured in a V-groove at 850 nm. The fiber has a core diameter of 5.3 μm and a relative index difference of 0.3 percent. No index matching.

The power transmission of light through a fiber coupling can be estimated by calculating the coupling between two Gaussian beams. Such estimations are adequate owing to the close match between Gaussian beams and the field distribution of single-mode fibers [8]. If we assume that we can neglect the loss due to separation between the two fiber ends, the coupling loss is given by [9]

$$CL = 10 \log \left[\left(\frac{2w_1 w_2}{w_1^2 + w_2^2} \right)^2 \cdot \exp \left\{ - \frac{2x^2}{w_1^2 + w_2^2} - \frac{2(\pi w_1 w_2 \theta)^2}{\lambda^2 (w_1^2 + w_2^2)} \right\} \right].$$

Here w_1 and w_2 are the beam spot sizes of the transmitting and receiving fibers, respectively. The lateral misalignment is given by x and the angular misalignment is given by θ. If we also neglect the variations in beam spot size along the fiber, the coupling loss formula reduces to

$$CL = 10 \log \left[\exp \left\{ - \left(\frac{x}{w} \right)^2 - \left(\frac{\pi \theta w}{\lambda} \right)^2 \right\} \right].$$

The single-mode fiber used in these experiments has a core diameter of 5.3 μm and a relative index difference of 0.3 percent. The measurements were done at 850 nm. Consequently, the beam spot size of the fiber is 3 μm [8]. Variations in the diameter and the circularity of the turned ferrules were found to be less than 0.05 μm. It is therefore realistic to assume that the maximum lateral misalignment is 0.2 μm. This lateral misalignment will cause a loss of 0.02 dB. Lateral misalignment caused by dust particles and errors in the V-groove is not included in the previous estimation. Since angular misalignments of less than 0.3° cannot be detected by the operator of the lathe, we can assume that the maximum angular misalignment in a coupling is 0.6°. Such angular misalignment will cause a coupling loss of 0.06 dB. Both misalignments can result in a loss of 0.08 dB. If we also add the measurement inaccuracy of 0.1 dB and the Fresnel reflection loss to the previous number, a value of 0.54 dB is obtained for the estimated maximum loss. This value is in reasonable agreement with the histograms shown in Fig. 10(a) and (b). The maximum loss indicated in the histogram of Fig. 10(c) cannot be explained, as one might expect, by the measurement inaccuracy and the ferrule inaccuracies alone because the sum of those is only 0.18 dB. However, the Fresnel reflection loss variation must be taken into account in this case. When one of the ferrules is rotated in steps, the reflection loss can vary between zero and the maximum value due to variations in the optical contact of the end surfaces [3]. Consequently, the maximum estimated value for this histogram is also 0.54 dB. Again, this is in reasonable agreement with the measured values.

Some limited tests were done using other materials for the ferrules and other types of single-mode fibers. The results are similar to those mentioned earlier.

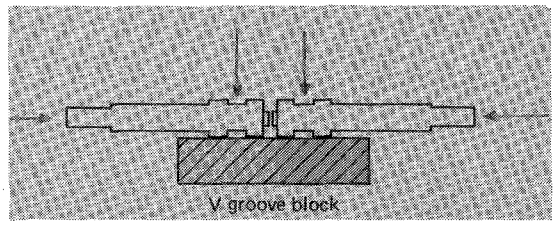

Fig. 11. Forces required for a proper coupling in a V-groove.

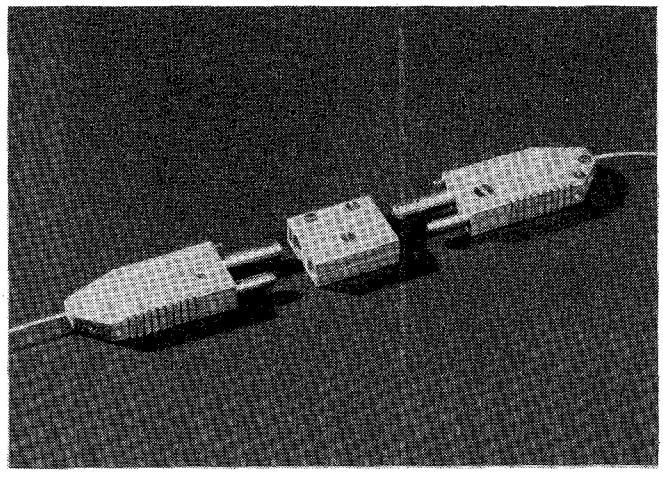

Fig. 12. Photograph showing two plugs and a central part.

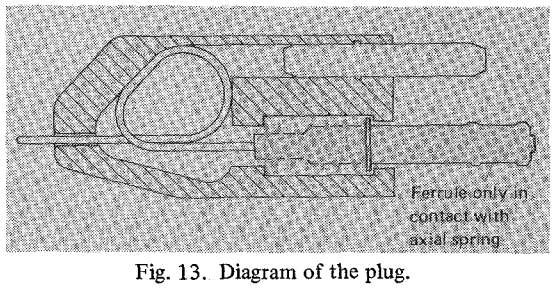

Fig. 13. Diagram of the plug.

V. Connector

Results of the previous tests initiated the design of a connector based on a simple V-groove in combination with provisions for securing and guiding the ferrules. Fig. 11 shows how the ferrules are placed in a V-groove and the forces that have to be applied. The axial forces are required to close the gap between the polished ends. The lateral force applied between the two rings, pointing to the bottom of the V-groove, secures the lateral position of the ferrule. This lateral force must be large enough to secure the ferrule in the V-groove in spite of mechanical vibrations.

The connector assembly is shown by the photograph in Fig. 12. It consists of three parts: a central coupling part containing the V-groove and two identical plugs containing the ferrules. The thickness of the system is 8 mm. The overall length of the three parts is 109 mm. The central part contains the V-groove and two lateral spring systems. The interior of this part will be explained later. The interior of the plug is shown in Fig. 13. The ferrule is only in contact with a conical coiled spring, which is used to apply the required axial force. This axial force is about 8 N. Separations of about 1 mm are present between the cylindrical surface of the ferrule and the rest of the plug. The ferrule can move laterally within those limits because the conical spring is very weak in this direction. The pin at the upper part of the plug serves to activate the lateral spring in the central part of the connector system when the plug is inserted. This pin also has a guiding function. Not shown in Fig. 13 is a spring lever that serves to lock the inserted plug to the central part.

Fig. 14 shows the successive stages of the connection procedure. Each lateral spring system in the central part consists of a light blade spring and a heavy blade spring. The light spring is aligned in such a way that it is in contact with the ferrule when the plug is inserted. In Fig. 14(b) the plug has been inserted half way. The ferrule is pushed forward by the coiled spring until it is blocked by a tiny pin in the middle of the V-groove. At this stage, the ferrule is laying properly in the V-groove due to the force applied by the light blade spring.

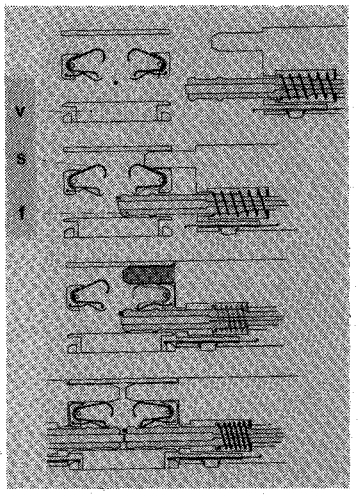

Fig. 14. Successive stages of the coupling procedure: (*v*) *V*-groove block; (*s*) lateral spring system; (*f*) ferrule.

The heavy blade spring has not yet been activated at this stage. Fig. 14(c) shows a plug which is completely inserted in the central part. The heavy spring is now activated because it is pushed down by the upper pin of the plug. The lateral forces of the spring system are 0.5 and 20 N, respectively. Fig. 14(d) shows both plugs inserted in the central part. When the second ferrule is inserted, it is blocked by the first ferrule which is already secured in the *V*-groove.

The lateral spring system in the central part has been divided into a heavy spring and a light spring to prevent unnecessary friction between the ferrule and the surface of the *V*-groove during the insertion procedure. A large lateral force is applied only when the ferrule is not in motion. When the plug is disconnected, the large lateral force will be released first due to retraction of the upper pin. Then the ferrule will start to move out. The light blade spring cannot be discarded because it ensures proper position of the ferrule in the *V*-groove before the large force is applied. This is important when the second ferrule is inserted. If the light spring is absent in this case, the front surface of the second ferrule will meet the other one prior to lateral alignment. When the heavy spring is activated in this situation, the ferrule is pushed toward the *V*-groove while the front surfaces are in contact. This procedure is obviously not favorable because of possible damage to the polished surfaces.

VI. Results and Conclusions

A histogram of coupling losses using the present connector is shown in Fig. 15. In this experiment, brass ferrules were used. The fiber was a single-mode fiber with a core diameter of 5.3 μm and relative index difference of 0.3 percent. All measurements were done at 850 nm without using index matching or coatings between the polished surfaces. The maximum connector loss measured in this batch was 0.56 dB and the average was 0.32 dB. These numbers can be compared with the previously calculated values. One of the connector assemblies was tested in a second experiment. The first plug of the assembly was connected and disconnected

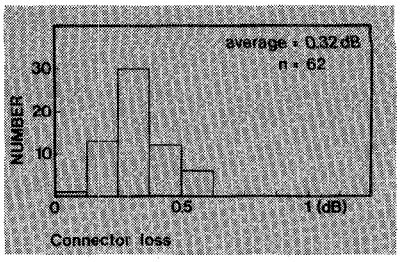

Fig. 15. Connector loss measured without index matching at 850 nm.

50 times and the same procedure was then repeated with the second plug. The coupling efficiency varies by no more than 2 percent of the original value of 0.3 dB.

The present results show that we have succeeded in the designing of a high-quality and reliable connector for single-mode fibers without using precision parts in the connector assembly. The present method allows some geometrical errors to be present in the fiber itself, such as core eccentricity and cladding size variations. Core size variation is one of the geometrical errors in the fiber which is not eliminated. This error could be the cause of the remaining connector loss. We are at present working to explain the connector losses by data of geometrical errors of the fiber which are not eliminated by the lathe.

The measurements presented in this section were done at 850 nm because misalignments have much more influence on the coupling losses between fibers at this wavelength than at 1300 nm wavelength. This can easily be seen by comparing calculated coupling losses for common single-mode fibers at 850 and 1300 nm, given in other papers [1], [2].

Acknowledgment

The authors are indebted to R. Cuppens and A. Verboven for their work on the fabrication and measurements and to A.J.J. Franken, J. Hagen, and C.J.T. Potters for useful advice. Thanks are also due to A.J.A. Nicia for comments on the manuscript.

References

[1] K. Nawata, "Multimode and single-mode fiber connectors technology," *IEEE J. Quantum Electron.*, vol. QE-16, pp. 618–627, June 1980.

[2] N. Suzuki, Y. Iwahara, M. Saruwatari, and K. Nawata, "Ceramic capillary connector for 1.3 micron single-mode fibres," *Electron. Lett.*, vol. 15, pp. 809–810, Dec. 1979.

[3] W. C. Young, P. Kaiser, N. K. Cheung, L. Curtis, R. E. Wagner, and D. M. Folkes, "A transfer-molded biconic connector with insertion losses below 0.3 dB without index match," in *Proc. 6th European Conf. on Opt. Commun.*, York, England, Sept. 16–19, 1980, pp. 310–314.

[4] G. D. Khoe, "New coupling techniques for single-mode fibres," in *Proc. 5th European Conf. on Opt. Commun.*, Amsterdam, The Netherlands, Sept. 17–19, 1979, pp. 6.1.1.–6.1.4.

[5] G. Kuyt, J. A. Luijendijk, G. D. Khoe, and H. G. Kock, "Metal sealed hermetic laser diode package suitable for direct single-mode fibre coupling," in *Proc. 7th European Conf. on Opt. Commun.*, Copenhagen, Denmark, Sept. 8–11, 1981, pp. P13.1–P13.4.

[6] J. W. Powell, *Design of Aerostatic Bearings.* London: Machinery, 1970.

[7] A.J.A. Nicia and A. Tholen, "High-efficient ball-lens connector and related functional devices for single-mode fibres," in *Proc. 7th European Conf. on Opt. Commun.*, Copenhagen, Denmark, Sept. 8–11, 1981, pp. 7.5.1.–7.5.4.

[8] D. Marcuse, "Loss analysis of single-mode fiber splices," *Bell Syst. Tech. J.*, vol. 56, May–June 1977, pp. 703–718.
[9] H. Kogelnik, "Coupling and conversion coefficients for optical modes," in *Quasi Optics, Microwave Research Institute Symposia Series.* Brooklyn, NY: Polytechnic Press, 1964, no. 14, pp. 333–347.

Giok-Djan Khoe (S'71–M'71) was born in Magelang, Indonesia, on July 22, 1946. He received the B.S. and M.S. degrees in electrical engineering from the Eindhoven University of Technology, Eindhoven, The Netherlands, in 1969 and 1971, respectively.

From 1972 to 1973 he worked on the laser diagnostics of plasmas at the FOM Institute of Plasma Physics Rijnhuizen, Nieuwegein, The Netherlands. In 1973 he joined Philips Research Laboratories, Eindhoven, The Netherlands, where he has worked on research and development of various optical waveguide devices. His main interests are the application of integrated optics and single-mode fiber technology. He is currently also engaged in the development of fiber guide local subscriber systems.

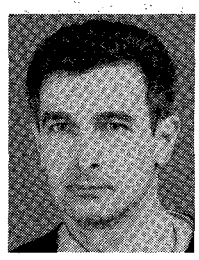

Johannes H.F.M. van Leest was born in Eindhoven, The Netherlands, on February 27, 1944. He received the certificate in mechanical engineering from Philips Vocational Training School, Eindhoven, The Netherlands, and the degree in precision mechanical engineering from the Polytechnic Institute, Eindhoven, The Netherlands, in 1961 and 1978, respectively.

In 1961 he joined Philips Research Laboratories, Eindhoven, The Netherlands, where he has worked on the design of high-precision mechanical devices. He is currently engaged in the development of interconnection devices for single-mode fibers.

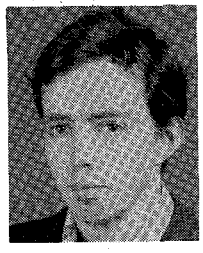

Johannes A. Luijendijk was born in Rotterdam, The Netherlands, on May 4, 1955. He received the degree in electrical engineering from the College of Advanced Technology, Rotterdam, The Netherlands, in 1978.

In 1979 he joined Philips Research Laboratories, Eindhoven, The Netherlands, where he has worked on various problems of optical waveguide technology.

The Nonlinear Coherent Coupler

STEPHEN M. JENSEN

Abstract—**This paper discusses the nonlinear coherent coupler (NLCC), a device useful for optical processing, but not bistable.**

This device utilizes the coherent interaction of two optical waveguides placed in close proximity. Because of the evanescent field overlap, these waveguides periodically exchange power. Nonlinear interactions modify the exchange of power and lead to strongly nonlinear transmission characteristics.

Introduction

RECENTLY, there has been great interest in the possibility of using optical devices for ultra-high-speed data processing. Many devices have been studied; of these the ones receiving the greatest attention are bistable optical devices [1]. Bistability, however, is not necessary in many logic operations. This paper discusses the nonlinear coherent coupler (NLCC), a device useful for optical processing, but not bistable.

This device, first described in 1980 [2], utilizes the coherent interaction of two optical waveguides placed in close proximity. Because of the evanescent field overlap, these waveguides periodically exchange power. Nonlinear interactions modify the exchange of power and lead to strongly nonlinear transmission characteristics which may be utilized in optical processing applications.

Fig. 1 shows a schematic of the NLCC device. The device is simply two waveguides placed adjacently so that they will couple to one another. The nonlinear material covers the region of interaction between the two waveguides. This nonlinearity may be due to the intrinsic nonlinearity of the substrate material, nonlinearity induced by doping of the substrate material, or by overlayers of highly nonlinear materials.

We have obtained an analytic solution for the NLCC response. To begin the analysis, we assume that the response of the medium, evident as a polarization, may be considered in two parts. The unperturbed linear portion $\bar{P}_o = 4\pi(\epsilon - 1)\bar{E}$ contains contributions from a single isolated waveguide. The perturbing polarization $\bar{P}'$ contains linear contributions from a waveguide placed in close proximity and nonlinear contributions due to the nonlinear response of the material. Using Maxwell's equations, in Gaussian units, one finds that

$$\bar{\nabla}_z \times \bar{E}_t(\bar{r}) + i\frac{c}{\omega}\bar{\nabla}_t \times \left\{\frac{1}{\epsilon}\bar{\nabla}_t \times \bar{H}_t(\bar{r})\right\} - i\frac{\omega}{c}\bar{H}_t(\bar{r}) = 4\pi\bar{\nabla}_t \times \frac{1}{\epsilon}\bar{P}'_z(\bar{r}) \quad (1)$$

and

Manuscript received March 1, 1982; revised June 16, 1982. This work was supported by the U.S. Air Force Avionics Laboratory under Contract F33615-79-C-1871.

The author is with Hughes Research Laboratories, Malibu, CA 90265.

0018-9480/82/1000-1568$00.75